Supporting Information

High effective and selective molecular nanowire catalysts for hydrogen and ammonia synthesis

Qian Wu,[a] Rui Peng,[a] Baibiao Huang,[a] Liangzhi Kou,[b] Ying Dai*[a] and Yandong Ma*[a]

[a]School of Physics, State Key Laboratory of Crystal Materials, Shandong University, Shandanan Str. 27, Jinan 250100, China

[b]School of Chemistry, Physics and Mechanical Engineering, Queensland University of Technology, Brisbane, Queensland, 4001, Australia

*Email: daiy60@sina.com (Y.D.); yandong.ma@sdu.edu.cn (Y.M.)

1. Methods

Formation energies (E_f) and dissolution potentials (U_{diss}) for TM atoms

$$E_f = E_{TM-Pc/PP} - E_{TM} - E_{Pc/PP}$$

where $E_{TM-Pc/PP}$, E_{TM} and $E_{Pc/PP}$ are the total energies of TM-Pc/PP nanowires, the chemical potential of single TM atom taken from its most stable bulk structure and the Pc/PP nanowires, respectively.

$$U_{diss} = U_{diss}^{'}(metal,bulk) - E_f/ne$$

where $U_{diss}^{'}(metal,bulk)$ is the standard dissolution potential of TM bulk, n is the number of electrons involved in the dissolution, and E_f is the formation energy of TM atoms.

HER mechanism

$$H^+ + e^- \rightarrow 1/2\ H_2\ (g)$$

The Gibbs free energy of hydrogen adsorption (ΔG_{H*})[1] under standard condition can be obtained by

$$\Delta G_{H*} = \Delta E_{H*} + \Delta E_{ZPE} - T\Delta S_H$$

where ΔE_H is the hydrogen adsorption energy, ΔE_{ZPE} and $T\Delta S_H$ are the zero-point energy difference and entropy difference between adsorbed H* atom and gas-phase H_2, respectively. In detail, ΔE_H, ΔE_{ZPE} and ΔS_H are given by

$$\Delta E_H = E_{H*} - E^* - \frac{1}{2}E_{H_2}$$

$$\Delta E_{ZPE} = E_{ZPE}^{H*} - \frac{1}{2}E_{ZPE}^{H_2}$$

$$\Delta S_H = S_{H*} - \frac{1}{2}S_{H_2}$$

where E_{H*}, E^*, and E_{H_2} are the energies of catalyst with one adsorbed H*, TM-Pc/PP, and gas-phase H_2, respectively. E_{ZPE}^{H*} and $E_{ZPE}^{H_2}$ are the zero-point energies of adsorbed H* without the contribution of catalyst and gas-phase H_2, respectively. S_{H*} and S_{H_2} represent the entropies of adsorbed H* atom and gas-phase H_2 at standard condition, respectively.

The entropy is given by[2]

$$S(T) = \sum_{i=1}^{3N}\left[-R\ln\left(1-e^{-\frac{hv_i}{k_BT}}\right) + \frac{N_A hv_i\ e^{-hv_i/k_BT}}{T\ \ 1-e^{-hv_i/k_BT}}\right]$$

where R stands for the universal gas constant, k_B is the Boltzmann constant, h is Plank's constant, N_A is Avogadro's number, v_i represents the frequency and N is the number of adsorbed atoms.

In the volcano curve, exchange current density i_0 is calculated as a function of ΔG_{H*} of hydrogen

adsorption according to Nørskov's assumption.[3] If $\Delta G_{H^*} \leq 0$, i_0 at pH = 0 is calculated as

$$i_0 = -ek_0 \frac{1}{1 + exp(-\Delta G_{H^*}/k_B T)}$$

If $\Delta G_{H^*} > 0$, i_0 is expressed as

$$i_0 = -ek_0 \frac{1}{1 + exp(\Delta G_{H^*}/k_B T)}$$

where k_0 is the rate constant and set to 1 here.

NRR mechanism

The Gibbs free energy of each elemental step (ΔG) of the NRR are adopted following the works of Nørskov et al.[4,5]

$$\Delta G = \Delta E + \Delta E_{ZPE} - T\Delta S + \Delta G_U + \Delta G_{pH}$$

where ΔE is the changed energy, ΔE_{ZPE} and ΔS are the change of zero point vibrational energy and the change of entropy, and can be obtained by the vibrational frequency of the optimized structures. T is the temperature and set to 298.15 K. The $\Delta G_U = -eU$, where e and U are the transferred charge and the electrode potential. ΔG_{pH} is the free energy correction of pH, which can be calculated by: $\Delta G_{pH} = k_B \times pH \times ln10$, where k_B is the Boltzmann constant and the value of pH is assumed to be zero.

The overpotentials (η) is expressed as follows:

$$\eta = U_{equilibrium} - U_{limiting}$$

where $U_{equilibrium} = -0.16$ V is the equilibrium potential of NRR and $U_{limiting} = -\Delta G/e$ is the limiting potential of the rate-limiting step, representing the required applied minimum potential to make the entire reaction spontaneous.

2. Supplementary Tables

Table S1. Calculated formation energies (E_f) and dissolution potentials (U_{diss}) of TM atoms, the spin moments (M) per cell of TM-Pc/PP nanowires, the energies of single TM atom in its most stable bulk structure and the standard dissolution potential of TM (TM = Ti-Zn) bulk. The corresponding single TM atoms energies (E_{TM}) of TM bulks and standard dissolution potentials ($U_{diss}^{'}$) of TM atoms are listed.

	TM-Pc			TM-PP			E_{TM}	$U_{diss}^{'}$
	E_f (eV)	U_{diss} (V)	M (μB)	E_f (eV)	U_{diss} (V)	M (μB)		
Ti	-6.21	3.11	2	-5.38	2.69	2	-7.77	-1.63
V	-5.60	2.80	3	-4.95	2.48	3	-8.94	-1.18
Cr	-5.90	2.95	4	-5.47	2.74	4	-9.51	-0.91
Mn	-4.60	2.30	3	-5.44	2.72	3	-8.88	-1.19
Fe	-4.79	2.40	2	-4.61	2.31	2	-8.31	-0.45
Co	-4.72	2.36	1	-4.61	2.31	1	-7.09	-0.28
Ni	-5.13	2.57	0	-5.11	2.56	0	-5.47	-0.26
Cu	-4.34	2.17	1	-3.96	1.98	1	-3.68	-0.34
Zn	-5.41	2.71	0	-4.75	2.38	0	-1.27	-0.76

Table S2. Computed Gibbs free energies (ΔG_{*N_2}), bond lengths of N-TM (d_{N-TM}) and N-N (d_{N-N}), charge transfers (ΔQ) of adsorbed N_2 with end-on and side-on adsorption configurations, and the hydrogen evolution free energies (ΔG_{H^*}) of TM-Pc nanowires (TM = Ti-Zn).

TM-Pc	end-on				side-on				ΔG_{H^*} (eV)
	ΔG_{*N_2} (eV)	d_{N-TM} (Å)	d_{N-N} (Å)	ΔQ (e^-)	ΔG_{*N_2} (eV)	d_{N-TM} (Å)	d_{N-N} (Å)	ΔQ (e^-)	
Ti	-0.62	2.03	1.121	0.26	-0.26	2.12	1.177	0.44	0.30
V	-0.42	1.95	1.119	0.23	0.24	2.21	1.148	0.26	0.51
Cr	0.40	3.01	1.114	0.01	1.22	2.08	1.163	0.32	0.35
Mn	0.38	2.42	1.118	0.02	0.42	2.40	-	-	0.44
Fe	0.12	1.76	1.126	0.26	0.11	1.77	-	-	0.27

Co	0.20	1.99	1.118	0.09	0.20	1.99	-	-	-0.07
Ni	0.43	3.19	1.114	0.06	0.42	3.15	-	-	1.79
Cu	0.43	3.14	1.113	-0.01	0.43	3.28	-	-	2.98
Zn	0.40	3.01	1.113	-0.02	0.43	3.29	-	-	1.54

Table S3. Computed Gibbs free energies (ΔG_{*N_2}), bond lengths of N-TM ($d_{N\text{-}TM}$) and N-N ($d_{N\text{-}N}$), charge transfers (ΔQ) of adsorbed N_2 with end-on and side-on adsorption configurations, and the hydrogen evolution free energies (ΔG_{H*}) of TM-PP nanowires (TM = Ti-Zn).

TM-PP	end-on				side-on				ΔG_{H*} (eV)
	ΔG_{*N_2} (eV)	$d_{N\text{-}TM}$ (Å)	$d_{N\text{-}N}$ (Å)	ΔQ (e^-)	ΔG_{*N_2} (eV)	$d_{N\text{-}TM}$ (Å)	$d_{N\text{-}N}$ (Å)	ΔQ (e^-)	
Ti	-0.44	2.03	1.134	0.35	0.01	2.15	1.168	0.37	2.90
V	-0.41	1.94	1.134	0.25	0.30	2.21	1.147	0.33	2.86
Cr	0.32	2.93	1.115	0.03	1.20	2.07	1.165	0.34	0.32
Mn	0.30	2.40	1.115	0.03	0.31	2.44	-	-	-0.57
Fe	0.00	1.73	1.135	0.24	0.02	1.74	-	-	0.34
Co	0.13	1.94	1.123	0.08	0.13	1.94	-	-	-0.04
Ni	0.42	3.13	1.114	0.00	0.42	3.13	-	-	1.40
Cu	0.42	3.11	1.114	-0.02	0.42	3.33	-	-	1.89
Zn	0.41	2.99	1.114	0.00	0.43	3.28	-	-	3.97

Table S4. Computated Faraday efficiency (FE) for Ti/Mo-Pc/PP nanowires.

	Ti-Pc	Ti-PP	Mo-Pc	Mo-PP
FE	0	100%	100%	97%

Table S5. Computated formation energies (E_f), dissolution potentials (U_{diss}) and spin moments (M) per cell for Mo-Pc/PP nanowires.

	Mo-Pc	Mo-PP
E_f (eV)	-3.87	-3.73
U_{diss} (V)	1.09	1.04

M (μB)	4.00	3.52

3. Supplementary Figures

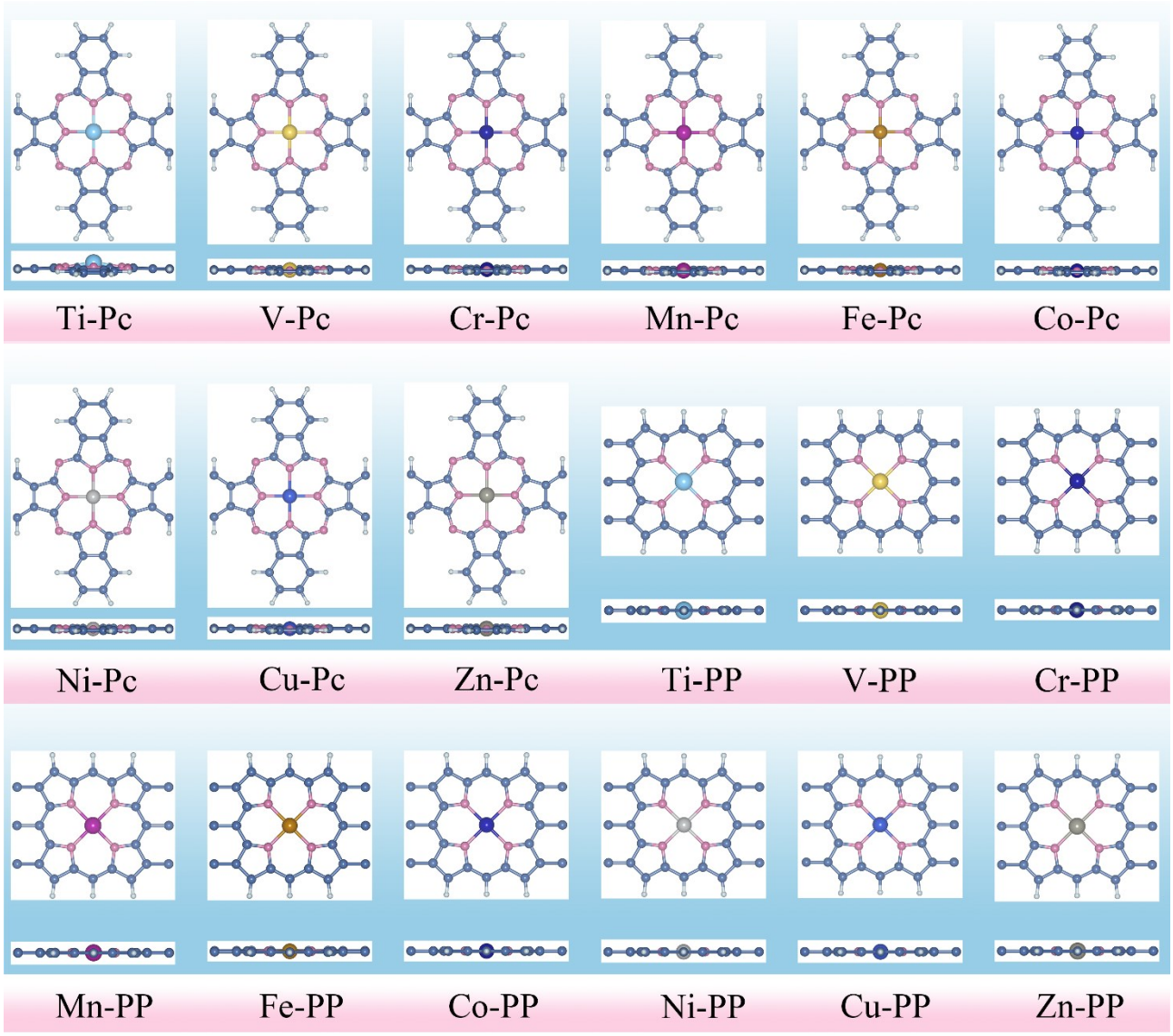

Figure S1. Crystal structures of the unit cell of TM-Pc/PP nanowires (TM = Ti-Zn).

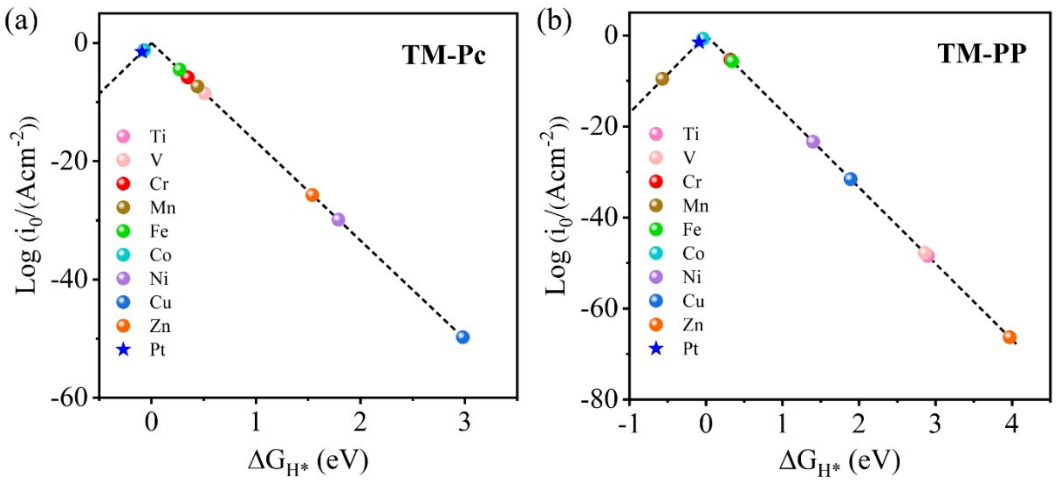

Figure S2. Volcano curve of exchange current (i_0) as a function of ΔG_{H^*} for (a) TM-Pc and (b) TM-PP nanowires (TM = Ti-Zn), and the volcano curve of Pt is also shown in for comparison.

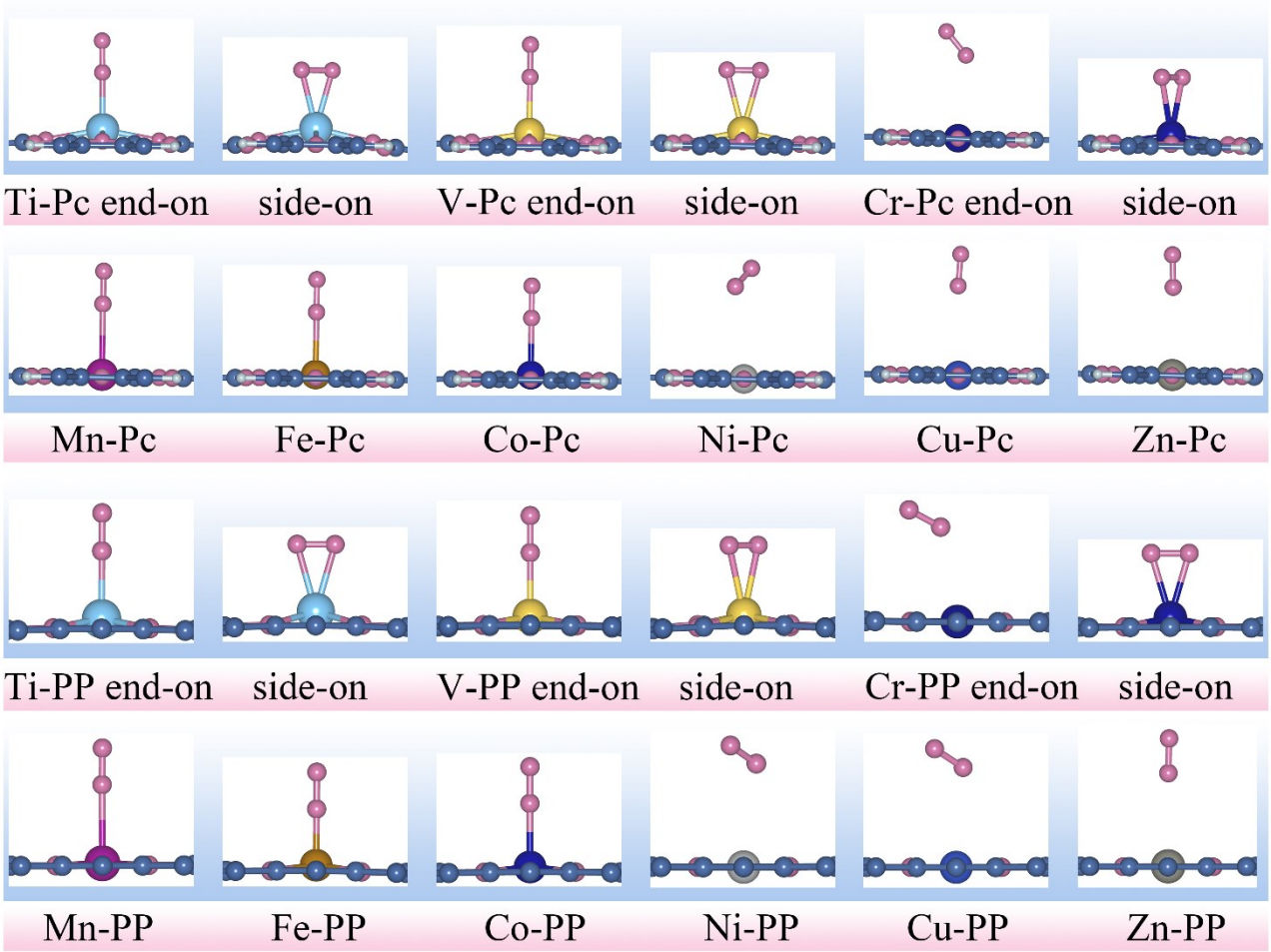

Figure S3. Crystal structures of N_2 adsorbed TM-Pc/PP nanowires with end-on and side-on configurations (TM = Ti-Zn).

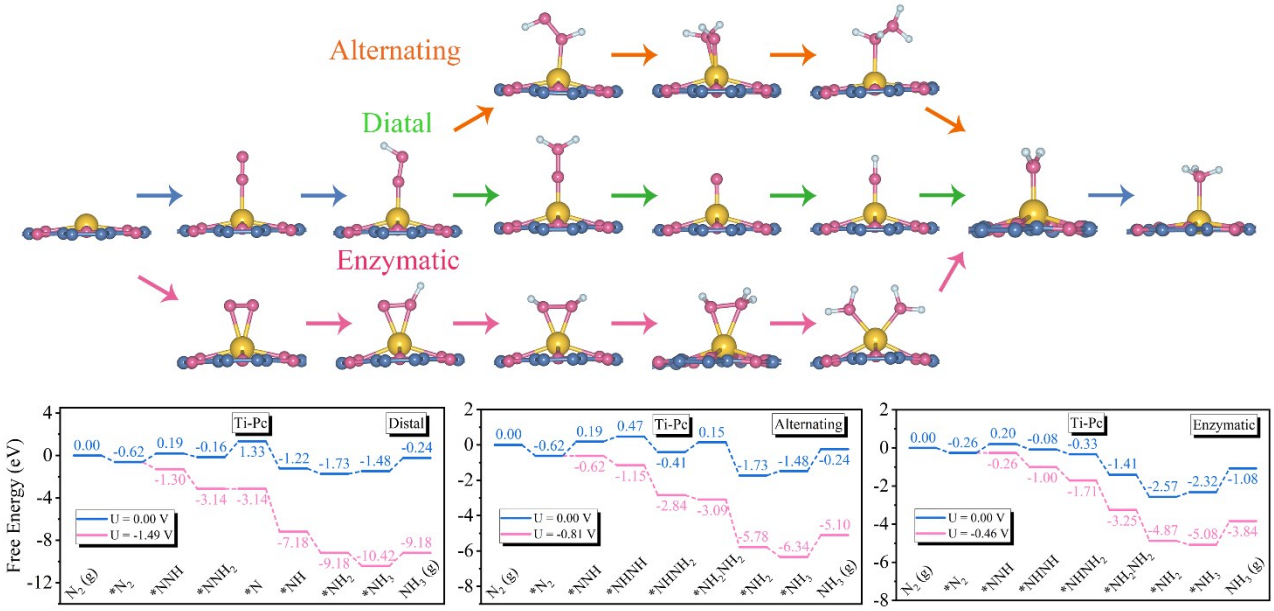

Figure S4. Crystal structures of various intermediates along the distal, alternating and enzymatic pathways of NRR on Ti-Pc nanowire. And the corresponding free-energy diagrams for the NRR process on Ti-Pc through distal, alternating, and enzymatic mechanisms.

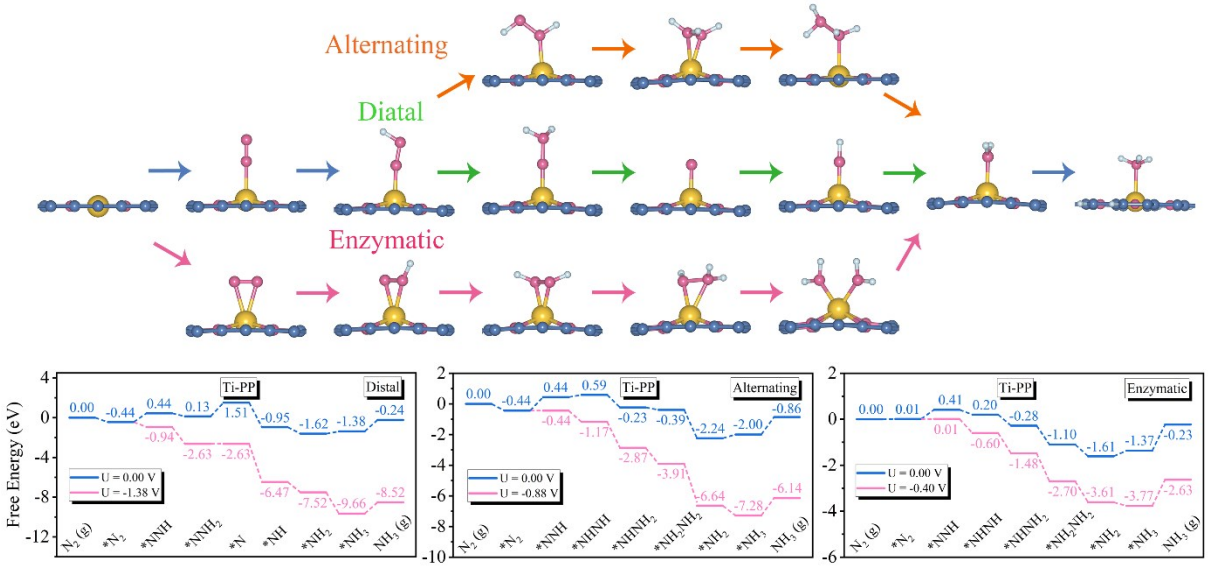

Figure S5. Crystal structures of various intermediates along the distal, alternating and enzymatic pathways of NRR on Ti-PP nanowire. And the corresponding free-energy diagrams for the NRR process on Ti-PP through distal, alternating, and enzymatic mechanisms.

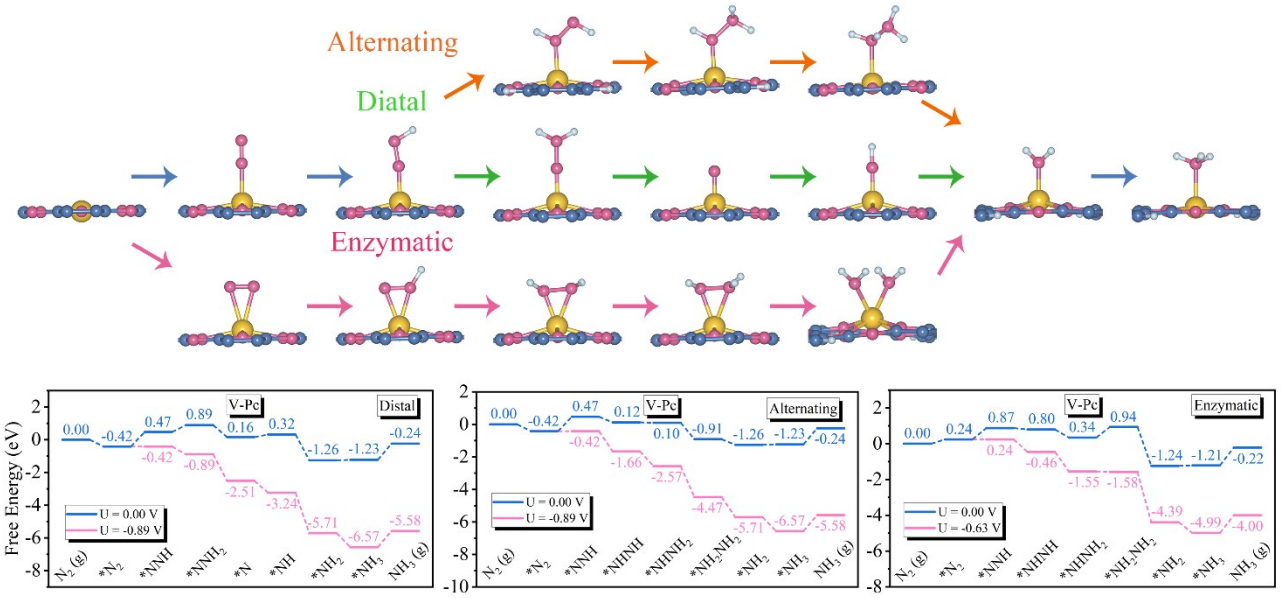

Figure S6. Crystal structures of various intermediates along the distal, alternating and enzymatic pathways of NRR on V-Pc nanowire. And the corresponding free-energy diagrams for the NRR process on V-Pc through distal, alternating, and enzymatic mechanisms.

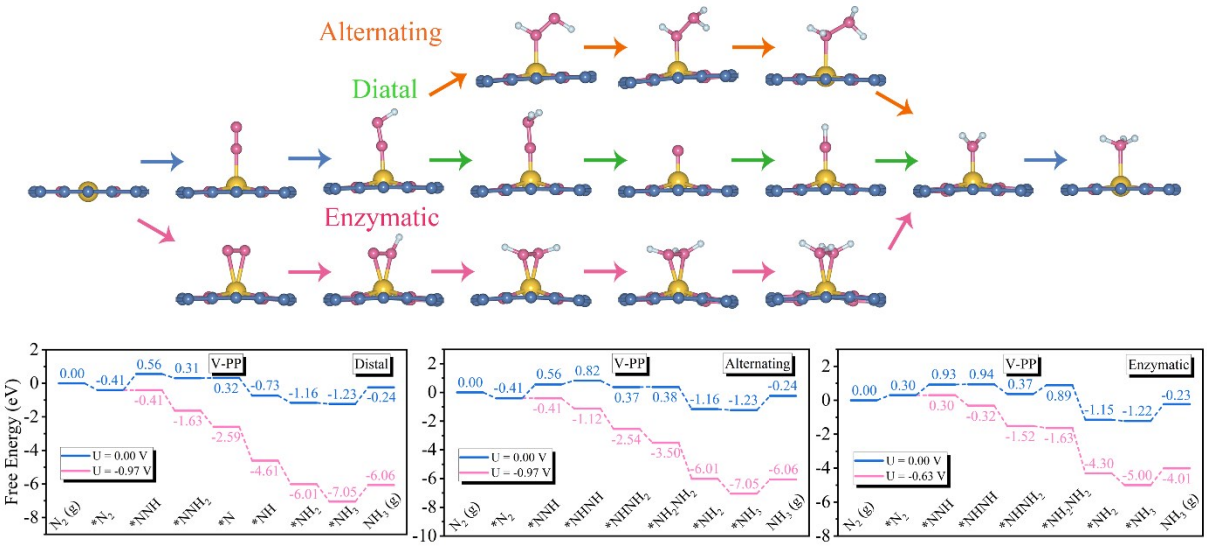

Figure S7. Crystal structures of various intermediates along the distal, alternating and enzymatic pathways of NRR on V-PP nanowire. And the corresponding free-energy diagrams for the NRR process on V-PP through distal, alternating, and enzymatic mechanisms.

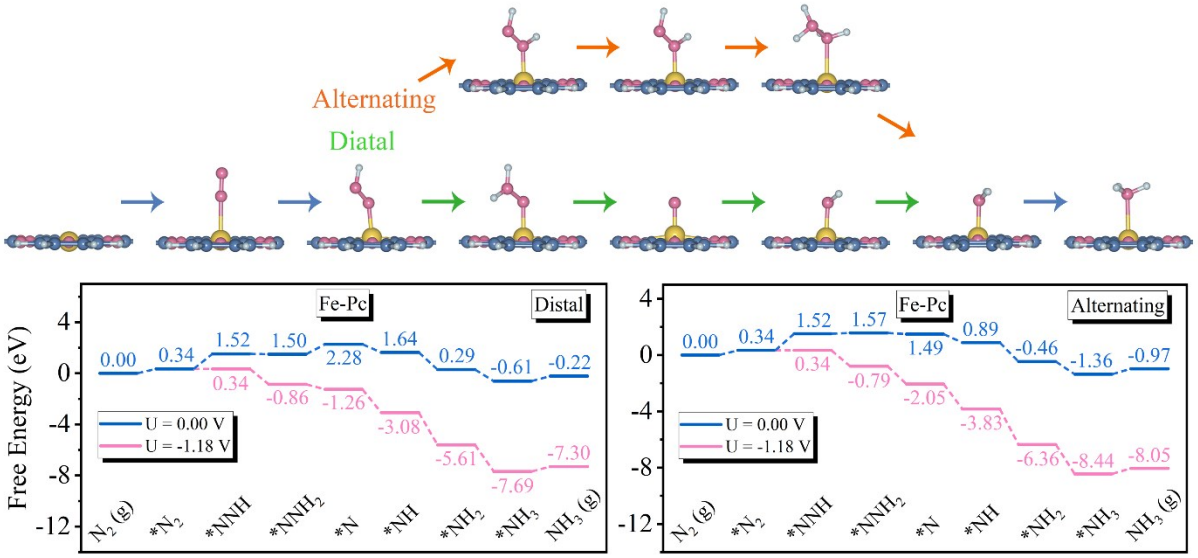

Figure S8. Crystal structures of various intermediates along the distal and alternating pathways of NRR on Fe-Pc nanowire. And the corresponding free-energy diagrams for the NRR process on Fe-Pc through distal and alternating mechanisms.

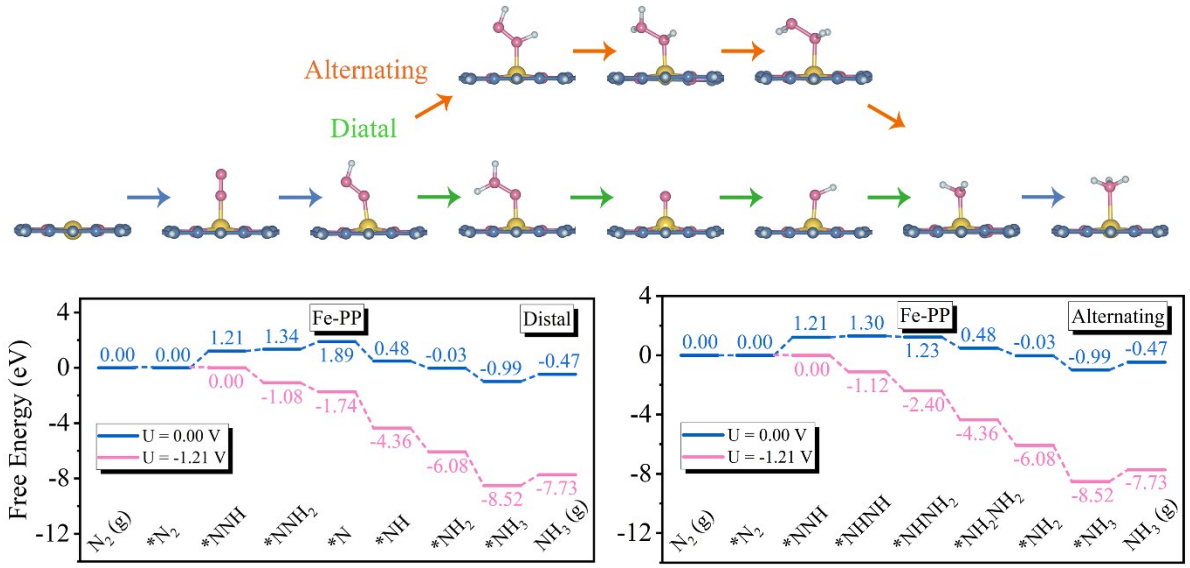

Figure S9. Crystal structures of various intermediates along the distal and alternating pathways of NRR on Fe-PP nanowire. And the corresponding free-energy diagrams for the NRR process on Fe-PP through distal and alternating mechanisms.

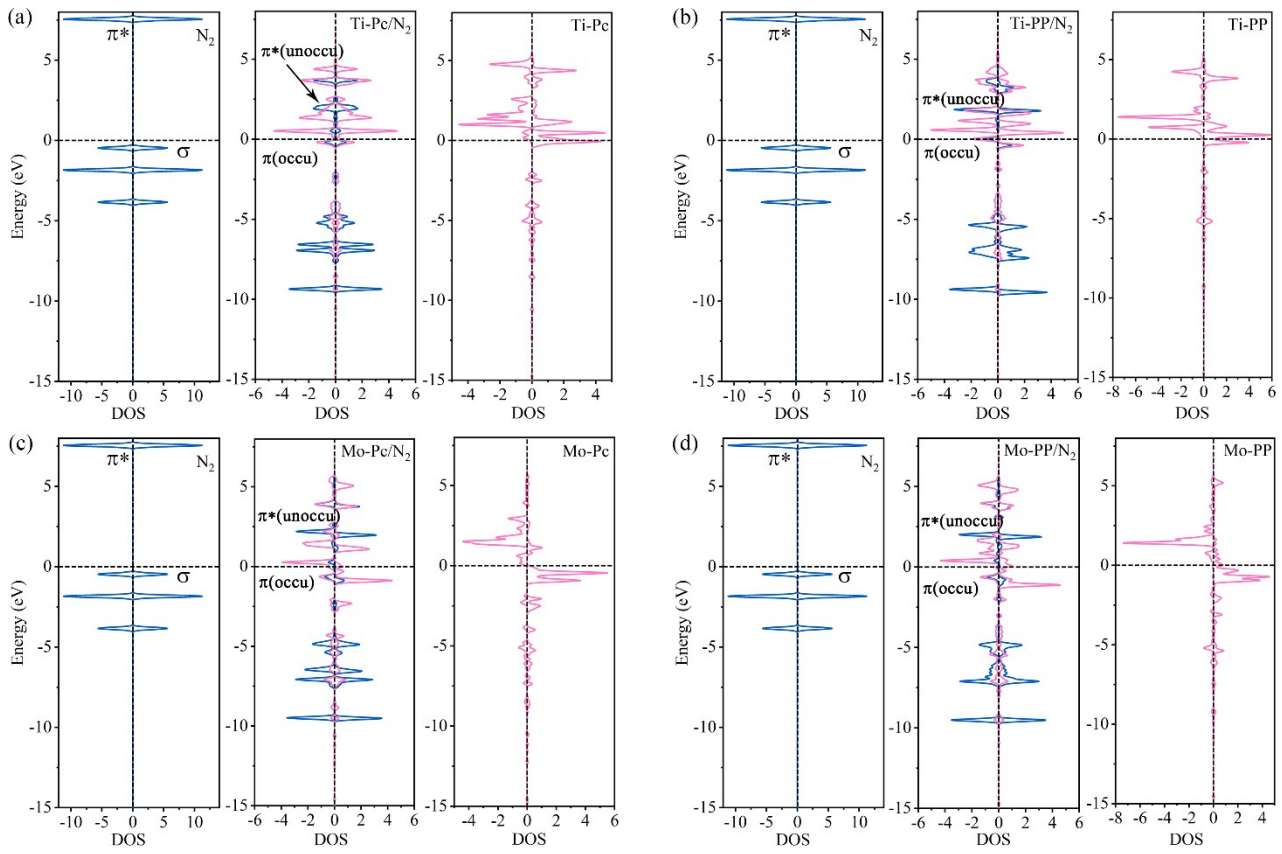

Figure S10. Projected density of states (PDOS) of free N_2, N_2 adsorption on Ti/Mo-Pc/PP and free Ti/Mo-Pc/PP.

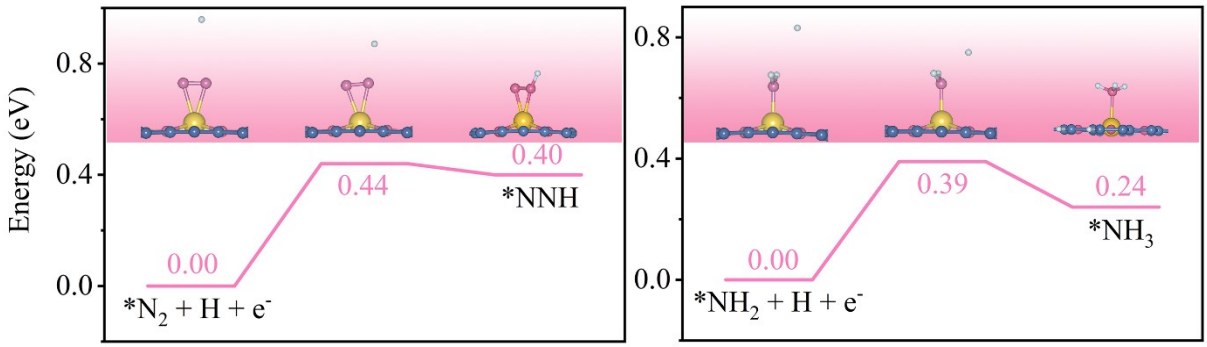

Figure S11. Crystal structures and related kinetic barriers of $*N_2$ and $*NH_2$ hydrogenation steps on Ti-PP nanowire.

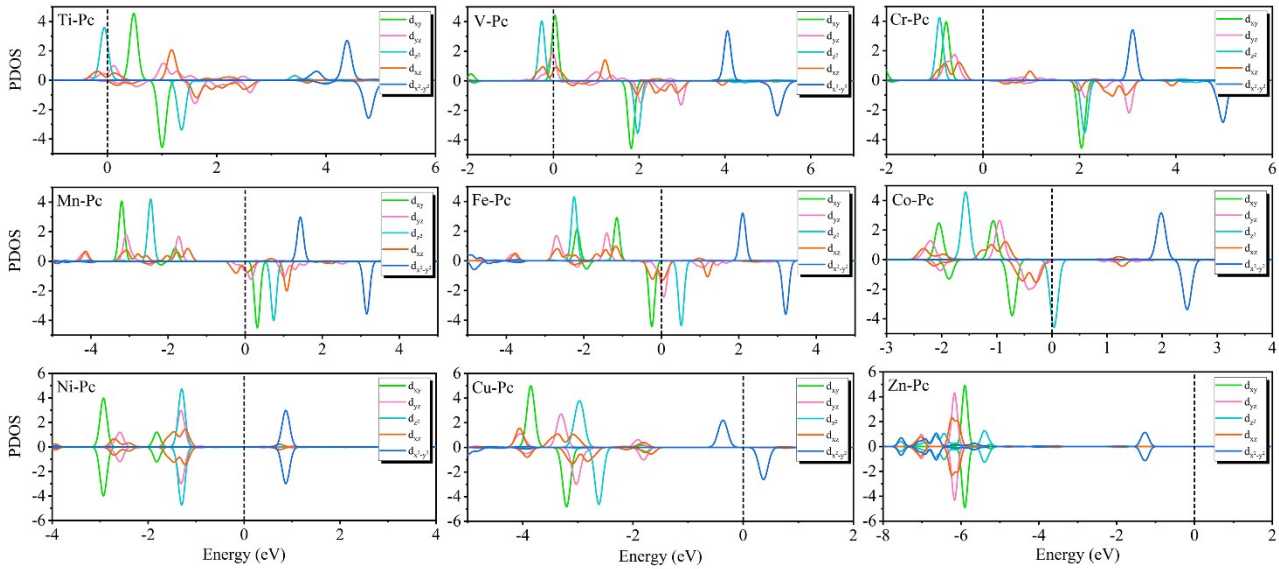

Figure S12. Computed projected density of states (PDOS) of d orbitals for TM-Pc nanowires (TM = Ti-Zn).

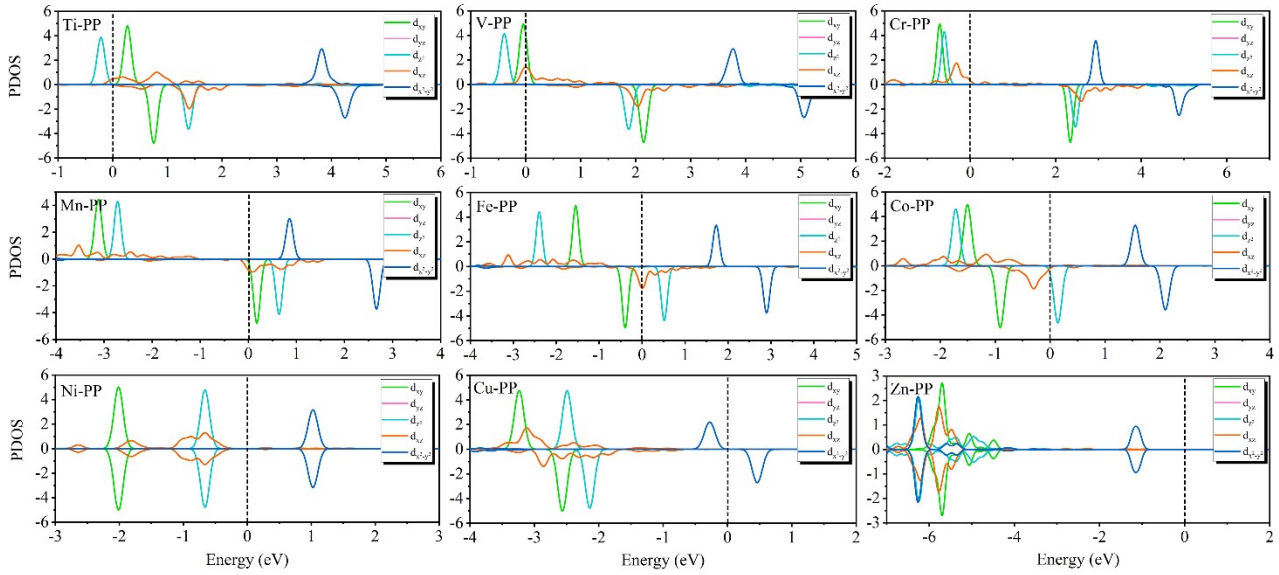

Figure S13. Computed projected density of states (PDOS) of d orbitals for TM-PP nanowires (TM = Ti-Zn).

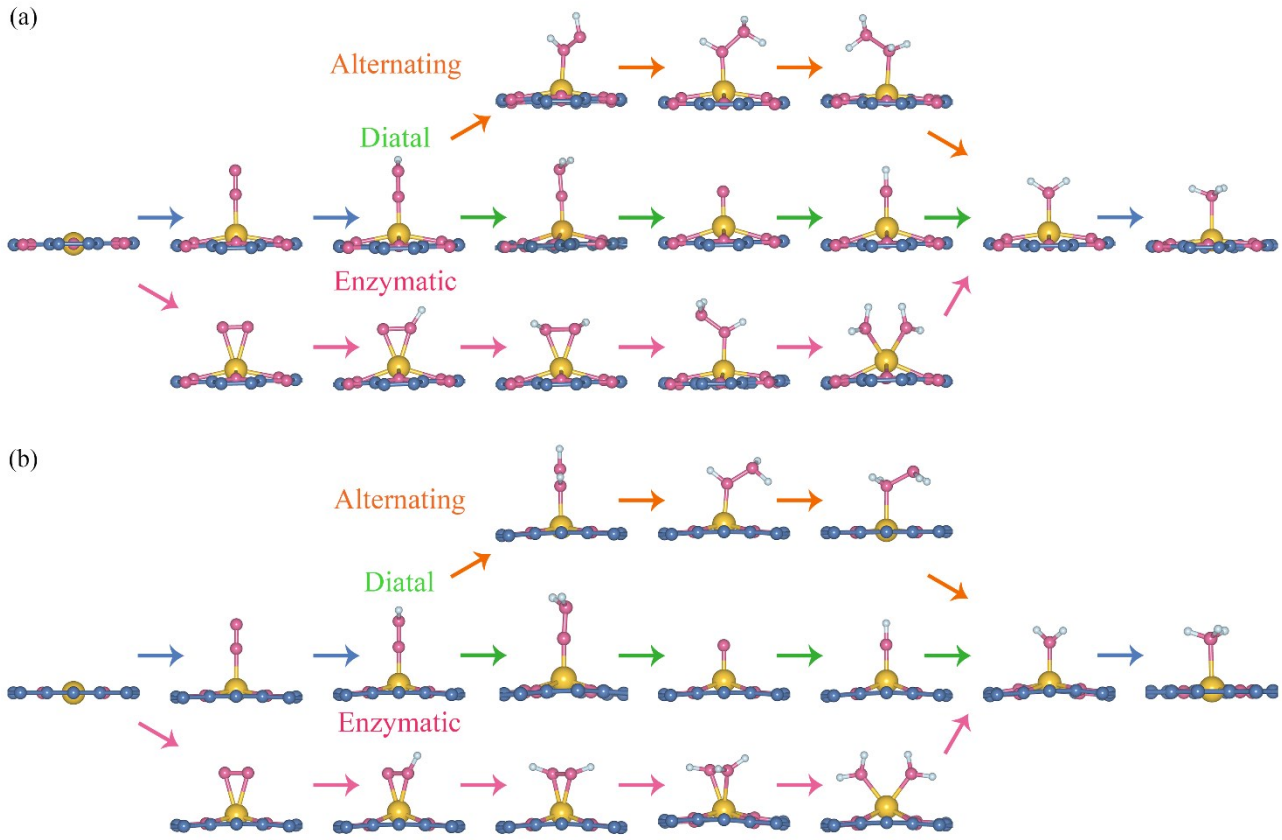

Figure S14. Crystal structures of various intermediates along the distal, alternating and enzymatic pathways of NRR on Mo-Pc and Mo-PP nanowires.

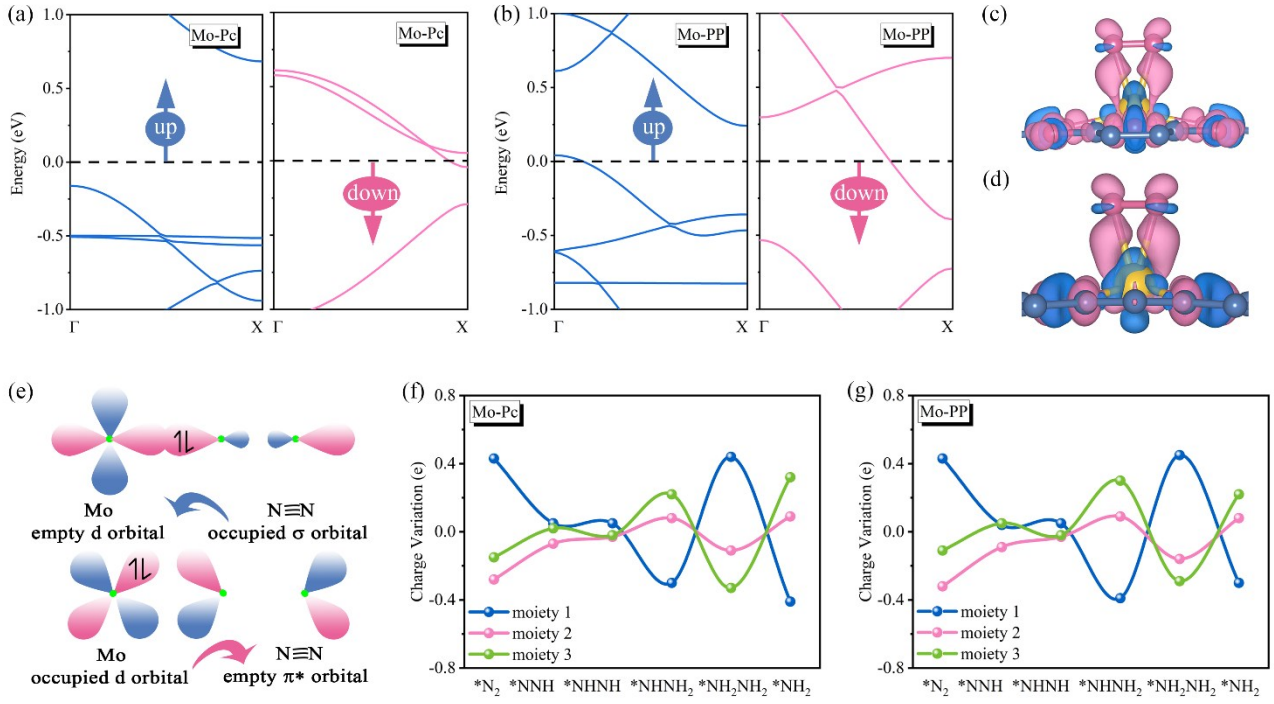

Figure S15. Band structures of (a) Mo-Pc and (b) Mo-PP, with blue (pink) lines indicating the majority (minority) spin channel. The Fermi level is set to zero. Charge density difference of N_2 adsorbed (c) Mo-Pc and (d) Mo-PP with side-on configuration. The isosurface value is set to be 0.01

e/Å^3, and positive (negative) charges are shown in pink (blue). (e) Simplified schematic of N_2 bonding to Mo atom. Charge variation of the three moieties for (f) Mo-Pc and (g) Mo-PP along the enzymatic pathway. Moieties 1, 2 and 3 in (f,g) indicate the *N_xH_y, Ti atom and Pc/PP, respectively.

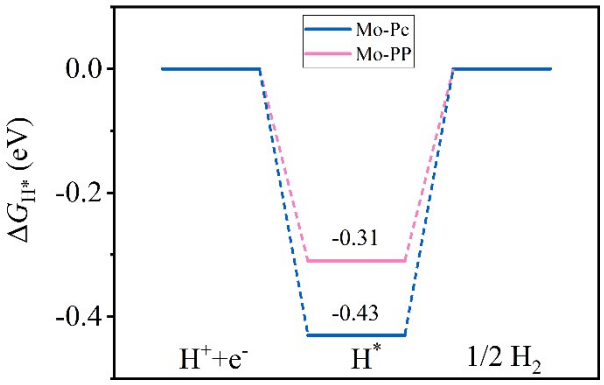

Figure S16. Gibbs free energy diagrams for the HER process of Mo-Pc and Mo-PP nanowires.

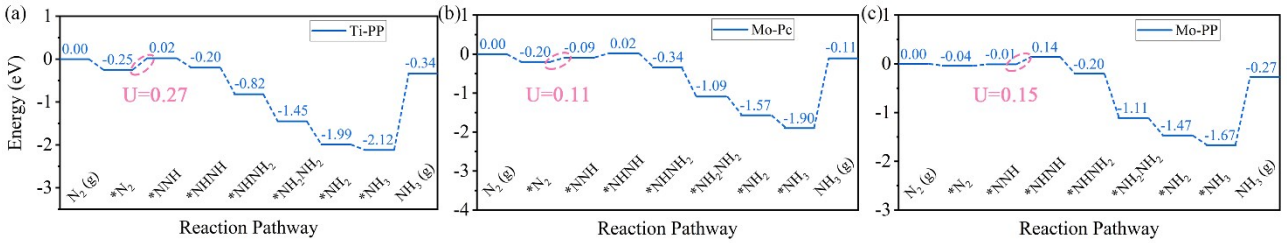

Figure S17. Gibbs free energy diagrams for the NRR process of Ti-PP and Mo-Pc/PP nanowires along the most preferred distal reaction pathway after considering the solvation effects.

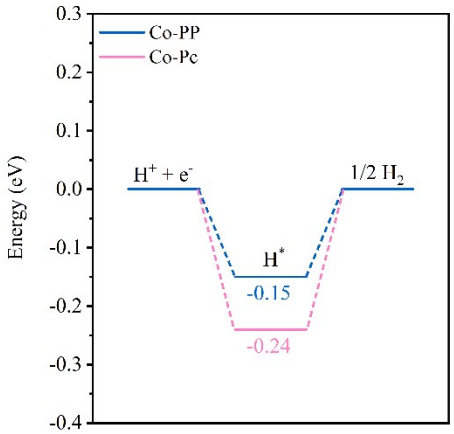

Figure S18. Gibbs free energy diagrams for the HER process of Co-Pc and Co-PP nanowires after

considering the solvation effects.

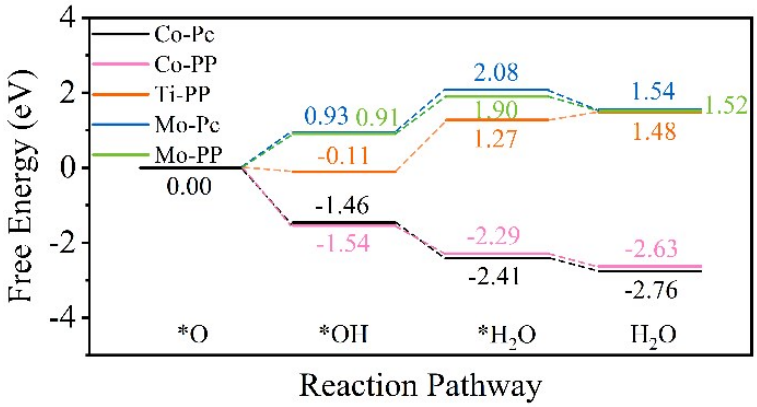

Figure S19. Relative free energy changes along the deoxidation/dehydroxylation process on the Ti-PP, Mo-Pc/PP and Co-Pc/PP surfaces at the potential of U = 0.

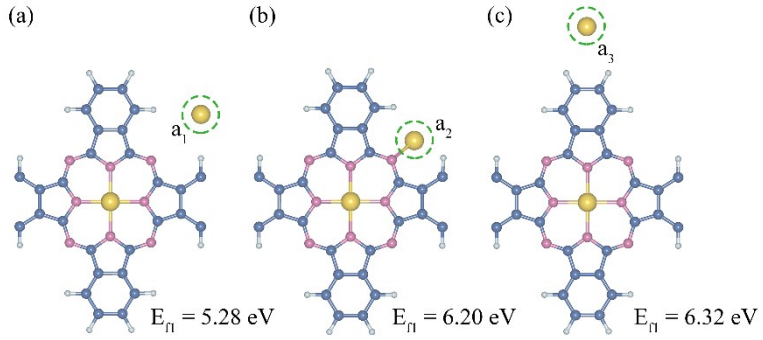

Figure S20. Possible anchoring sites of Mo atom on the edge of Mo-Pc nanowires. The corresponding formation energies are included.

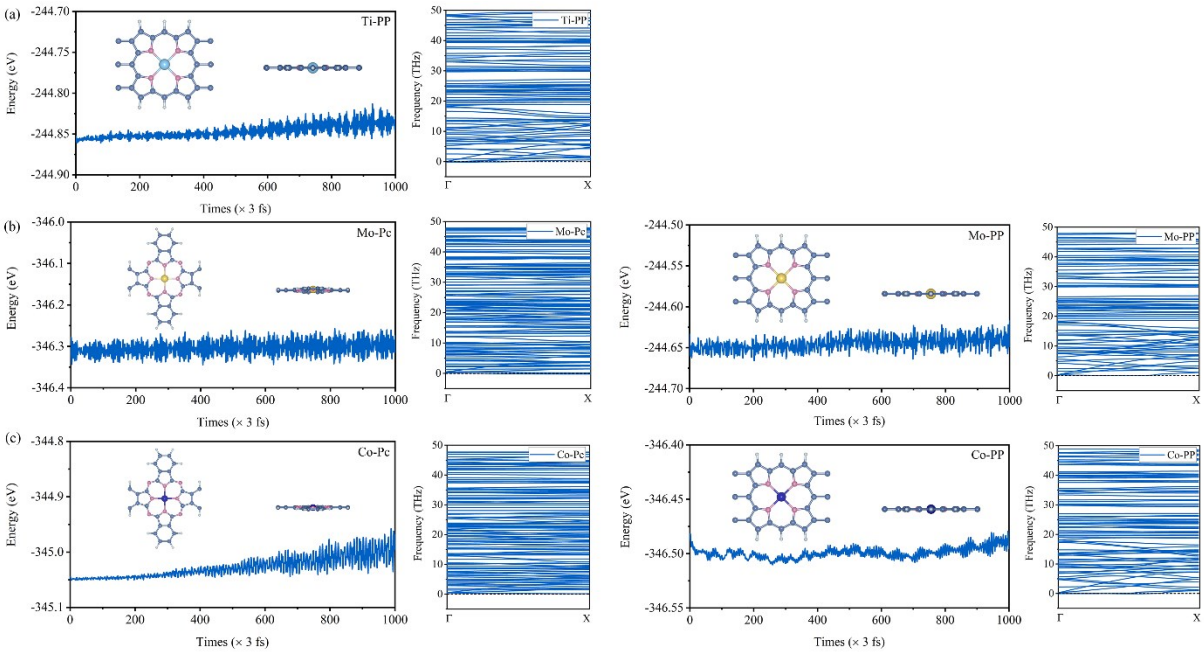

Figure S21. Phonon dispersion spectra and the total energy as a function of time at 300 K during AIMD simulations for (a) Ti-PP, (b) Mo-Pc/PP and (c) Co-Pc/PP nanowires. Insets are structures after 3 ps AIMD simulations.

4. References

(1) C. Tsai, F. Abild-Pedersen and J. K. Nørskov, *Nano Lett.*, 2014, **14**, 1381−1387.

(2) Y. A. Zhu, D. Chen, X. G. Zhou and W. K. Yuan, *Catal. Today*, 2009, **148**, 260–267.

(3) J. K. Nørskov, T. Bligaard, A. Logadottir, J. R. Kitchin, J. G. Chen, S. Pandelov and U. Stimming, *J. Electrochem. Soc.*, 2005, **152**, J23−J26.

(4) J. K. Nørskov, J. Rossmeisl, A. Logadottir, L. Lindqvist, J. R. Kitchin, T. Bligaard and H. J. K. Jonsson, *J. Phys. Chem. B*, 2004, **108**, 17886−17892.

(5) A. A. Peterson, F. Abild-Pedersen, F. Studt, J. Rossmeisl and J. K. Nørskov, *Energy Environ. Sci.*, 2010, **3**, 1311−1315.